Rosa Vono,[1] Claudia Fuoco,[2] Stefano Testa,[2] Stefano Pirrò,[2] Davide Maselli,[1,3] David Ferland McCollough,[4] Elena Sangalli,[1] Gianfranco Pintus,[3,5] Roberta Giordo,[3] Giovanna Finzi,[6] Fausto Sessa,[6] Rosanna Cardani,[7] Ambra Gotti,[1] Sergio Losa,[1] Gianni Cesareni,[2] Roberto Rizzi,[1,8] Claudia Bearzi,[1,8] Stefano Cannata,[2] Gaia Spinetti,[1] Cesare Gargioli,[2] and Paolo Madeddu[3]

Activation of the Pro-Oxidant PKCβII-p66^{Shc} Signaling Pathway Contributes to Pericyte Dysfunction in Skeletal Muscles of Patients With Diabetes With Critical Limb Ischemia

Diabetes 2016;65:3691–3704 | DOI: 10.2337/db16-0248

Critical limb ischemia (CLI), foot ulcers, former amputation, and impaired regeneration are independent risk factors for limb amputation in subjects with diabetes. The present work investigates whether and by which mechanism diabetes negatively impacts on functional properties of muscular pericytes (MPs), which are resident stem cells committed to reparative angiomyogenesis. We obtained muscle biopsy samples from patients with diabetes who were undergoing major limb amputation and control subjects. Diabetic muscles collected at the rim of normal tissue surrounding the plane of dissection showed myofiber degeneration, fat deposition, and reduction of MP vascular coverage. Diabetic MPs (D-MPs) display ultrastructural alterations, a differentiation bias toward adipogenesis at the detriment of myogenesis and an inhibitory activity on angiogenesis. Furthermore, they have an imbalanced redox state, with downregulation of the antioxidant enzymes superoxide dismutase 1 and catalase, and activation of the pro-oxidant protein kinase C isoform β-II (PKCβII)-dependent p66^{Shc} signaling pathway. A reactive oxygen species scavenger or, even more effectively, clinically approved PKCβII inhibitors restore D-MP angiomyogenic activity. Inhibition of the PKCβII-dependent p66^{Shc} signaling pathway could represent a novel therapeutic approach for the promotion of muscle repair in individuals with diabetes.

Critical limb ischemia (CLI) represents the most severe manifestation of peripheral arterial disease and the major cause of foot amputation in the U.S. (1). Most amputations are performed on people with diabetes, who have rampant atherosclerosis and poor angiomyogenesis (2–5).

Satellite cells and pericytes, which reside on opposite sides of the myofiber basement membrane, represent the main myogenic stem/progenitor cells in postnatal skeletal muscle (6). Satellite cells are well-acknowledged targets of diabetes-induced damage and are contributors of diabetic vascular myopathy (7–10). Recent evidence indicates that pericytes play a key role in vascular and muscular regeneration (11–13) and have the potential to become favorite candidates for cell therapy for peripheral arterial disease and myocardial ischemia (14–17). However, to the best of our knowledge, no investigation has assessed the impact of diabetes on the functional and molecular makeup of muscular pericytes (MPs).

[1]Istituto di Ricovero e Cura a Carattere Scientifico, MultiMedica, Milan, Italy
[2]Department of Biology, University of Rome Tor Vergata, Rome, Italy
[3]Department of Biomedical Sciences, University of Sassari, Sassari, Italy
[4]Bristol Heart Institute, University of Bristol, Bristol, U.K.
[5]Department of Biomedical Sciences, College of Health Sciences, Qatar University, Doha, Qatar
[6]Department of Pathology, University of Insubria/Ospedale di Circolo, Varese, Italy
[7]Laboratory of Muscle Histopathology and Molecular Biology, Istituto di Ricovero e Cura a Carattere Scientifico-Policlinico San Donato, Milan, Italy
[8]Cell Biology and Neurobiology Institute, National Research Council of Italy, Rome, Italy

Corresponding authors: Paolo Madeddu, paolo.madeddu@bristol.ac.uk, Cesare Gargioli, cesare.gargioli@uniroma2.it, and Gaia Spinetti, gaia.spinetti@multimedica.it.

Received 22 February 2016 and accepted 24 August 2016.

This article contains Supplementary Data online at http://diabetes.diabetesjournals.org/lookup/suppl/doi:10.2337/db16-0248/-/DC1.

The mitochondrial adaptor protein Shc1, isoform p66 ($p66^{Shc}$), a redox enzyme that triggers mitochondrial apoptosis, is implicated in the pathophysiology of aging and cardiovascular disease (18–20). Studies in experimental models suggest that modulation of $p66^{Shc}$ expression and activity may be a novel and effective target for the treatment of cardiovascular complications. For instance, abrogation of $p66^{Shc}$ results in protection from angiotensin II–induced cardiomyocyte damage (21), improvement of neovascularization and muscle fiber survival after induction of limb ischemia, and preservation of proliferation and differentiation of satellite cells exposed to high oxidative stress (22,23). Upstream modulators of the $p66^{Shc}$ signaling pathways, such as the protein kinase C isoform β-II (PKCβII), which activates $p66^{Shc}$ through phosphorylation of its serine 36 residue at the COOH-terminal moiety, also represent an attractive therapeutic target to halt ischemic complications (20,24). After successful use in diabetic animals, the PKCβII inhibitor LY333531, also known as Ruboxistaurin, has recently shown a clear therapeutic benefit in clinical trials of diabetic microvascular complications (25,26). However, whether PKCβII inhibitors exert positive effects on myogenic stem cells from patients with diabetes with vasculopathy currently remains unknown.

The current study investigates molecular therapeutic targets to improve angiomyogenesis in patients with complicated diabetes. We assessed functional and molecular features of MPs harvested at the rim of tissue above the plane of limb amputation, which is a rescuable area similar to the peri-infarct border zone. We show for the first time that diabetic MPs (D-MPs) are dysfunctional in many respects. They have a reduced capacity to expand in culture, differentiate into multinucleated myotubes, and support endothelial cells (ECs) network formation. Furthermore, an increased oxidative stress is recurrent in D-MPs, due to the downregulation of superoxide dismutase 1 (SOD-1) and catalase, and upregulation and activation of $p66^{Shc}$. Importantly, blockade of $p66^{Shc}$ phosphorylation by PKCβII inhibition restores D-MP functionality, providing a novel indication for molecular treatment of the angiomyogenic pathology in patients with diabetes.

RESEARCH DESIGN AND METHODS

Human Studies

Skeletal muscle biopsy samples were obtained from control subjects and patients with diabetes after informed consent was given, in line with the guidelines on human rights of the Declaration of Helsinki. MPs were isolated from the following: *1*) different anatomic locations of the lower extremities from control subjects, referring to our institutions for investigations/therapeutic interventions related to leg varicosity or suspected bone-related pathologies that then resulted in negative findings (n = 14); or *2*) sartorius muscles from patients with type 2 diabetes at the occasion of major amputation for CLI (n = 18). CLI was diagnosed according to Trans-Atlantic Inter-Society Consensus Document on Management of Peripheral Arterial Disease (TASC) 2007 guidelines (i.e., rest for pain and/or ulcer or gangrene, transcutaneous oximetry at the dorsum of the foot of <30 mmHg, and/or ankle pressure of <70 mmHg). Patient characteristics are listed in Table 1. We attempted to perform all of the analyses on the same sample. When this was not possible because of the small size of the harvested tissue, priority was given to histological analyses and then to the proliferation assay. Supplementary Table 1 summarizes the attribution of samples to different assays.

Muscle Immunohistochemistry

Morphometric analysis was performed on hematoxylin-eosin–stained sections. For capillary analysis, sections were boiled in sodium citrate buffer, pH 6.0, incubated with mouse monoclonal anti-CD31 antibody clone CJ70A (1:200; Dako), then washed and incubated with secondary antibody followed by DAB+ substrate 1:50 (REAL EnVision Kit; Dako). Analysis of inflammatory infiltrates used rabbit monoclonal anti-CD3 (clone 2GV6) and mouse monoclonal anti-CD68 (clone PG-M1) antibodies (both from Ventana). To localize MPs within the muscle structure, cryosections were treated with an alkaline phosphatase (ALP) staining solution containing nitro-blue tetrazolium chloride (160 μg/mL) and 5-bromo-4-chloro-3′-indolyphosphate p-toluidine salt (300 μg/mL; both from Sigma-Aldrich) in ALP buffer (100 mmol/L TrisHCl, 150 mmol/L NaCl, and 1 mmol/L $MgCl_2$, pH 9.0). The same solution was used to stain isolated cells previously fixed in 2% formalin. ALP quantification in

Table 1—Characteristics of the study populations

	Control subjects (n = 14)	Patients with diabetes (n = 18)	P value
Age (years ± SEM)	70 ± 3	75 ± 2	0.1
Male sex (%)	54	67	0.2
Time of known diabetes (years ± SEM)	0	17.2 ± 3.2	
HbA_{1c} [% ± SEM (mmol/mol ± SEM)]	n.a.	7.4 ± 0.5 (63.2 ± 4.3)	
Glycemia (mmol/L ± SEM)	5.4 ± 0.4	8.8 ± 1.6	0.02
Creatinine (μmol/L ± SEM)	91.3 ± 11	132.4 ± 35	0.9

n.a., not applicable.

cryosections was performed using Cell Profiler open source software distributed under a GPLv2 public license.

Myofiber Cross-sectional Analysis

Cryosections from diabetic and control muscle biopsy samples were stained with antilaminin antibody and analyzed using an ImageJ macro. For each sample (n = 3), an area of >2,000 single fibers was measured.

MP Isolation

Human MPs were isolated after well-established procedures (12,27). Briefly, muscle biopsy samples were finely minced and digested with collagenase II (100 units/mL) for 45 min at 37°C with shaking. The digestion mixture was centrifuged and resuspended in growth medium (α-minimum essential medium supplemented with 20% FBS). The cell suspension was filtered through a 70-μm cell strainer, dispensed in plastic dishes at clonal density (1,000 cell/cm^2), and incubated at 37°C with 5% CO_2 in the growth medium. MPs were selected by plastic adherence in culture for at least 10 days when they form colonies positive for ALP, neural/glial antigen 2 (NG2), and CD146 (27).

Transmission Electron Microscopy

For ultrastructural analysis, a pellet of MPs was fixed for 2 h at 4°C in a mixture of 2% paraformaldehyde (PFA) and 2% glutaraldehyde in 0.05 mol/L, pH 7.3, cacodylate buffer; postfixed in 1% osmium tetroxide; and embedded in epon-Araldite. Thin sections were counterstained with uranyl acetate and lead citrate, and examined with a Philips/FEI Morgagni electron microscope.

Immunocytochemistry

After fixation with 4% PFA, cells were permeabilized with 0.3% Triton X-100 in PBS 1× plus 1% BSA, then blocked with goat serum 10% in PBS 1×; and incubated with polyclonal rabbit anti-NG2 (Merck Millipore), mouse monoclonal anti-CD146 (clone OJ79c; Abcam), mouse monoclonal antidesmin (clone D33; Dako), mouse monoclonal anti-MyHC (clone MF20; Developmental Studies Hybridoma Bank), and mouse monoclonal anti-Ser36-phospho-p66^{Shc} (clone 6E10; Abcam); and diluted following the manufacturer instructions. Cells were further incubated with goat anti-mouse or anti-rabbit fluorescent secondary antibodies (Alexa Fluor 488 or 555; Life Technologies). Nuclei were counterstained with DAPI (PanreacAppliChem). Microphotographs were acquired using the imaging software AxioVision Imaging System (Zeiss, Jena, Germany). When required for three-dimensional image acquisition, an Olympus FV 1000 confocal laser scanning microscope with a 60× oil-immersion lens was used.

MP Flow Cytometry

MPs were stained for surface antigen expression using the following antibodies: CD44-APC, CD90-APC, and ALP-PerCP Cy5.5 (all from BD Biosciences). For Ser36-phospho-p66^{Shc} quantification, cells were fixed and permeabilized using BD Citofix/Citoperm kit (BD Biosciences). They were then incubated with anti-Ser36-phospho-p66^{Shc} (Abcam), followed by Alexa Fluor 633–conjugated secondary antibody. Fluorescence was analyzed on a FACSCanto flow cytometer using the FACSDiva software (BD Biosciences), setting a nonlabeled population as a negative control.

Myogenic Differentiation

MPs were seeded at 10^5 cells/well in two-well glass chamber slides and were expanded in culture for 7 days to allow cell fusion and myotube formation. Cells were fixed with 4% PFA and permeabilized with 0.3% Triton X-100 in 1% BSA. Myogenic differentiation and myotube formation were assessed by staining cells with anti–myosin heavy chain (MyHC) antibody (clone MF20; Developmental Studies Hybridoma Bank), followed by Alexa Fluor 555–conjugated secondary antibody.

Adipogenic Differentiation

MPs were induced to differentiate into adipocytes using an inductive medium for 4 days (i.e., DMEM GlutaMAX high-glucose, 1% penicillin and streptomycin, 1% sodium pyruvate supplemented with 20% FBS, and insulin [1 μg/mL]). Adipogenic differentiation was assessed by Oil Red O staining (Sigma-Aldrich) after PFA fixation.

Proliferation Assay

MP proliferation was assessed by ELISA BrdU colorimetric assay kit (Roche). Briefly, cells (10^3 cells/well in a 96-well microplate in triplicate) were grown for 24 h and then treated with BrdU (10 μmol/L final concentration) for an additional 24 h. The colorimetric reaction was stopped by adding H_2SO_4 (250 mmol/L final concentration) and read immediately at 450 nm.

EC Network Assay

Human umbilical vein ECs (HUVECs) and MPs were seeded in an eight-well Permanox chamber slide (Nunc) coated with Matrigel (3D; BD Biosciences) alone (3.75×10^4 cells/well) or cocultured at 1:4 ratio (MPs to HUVECs) in EBM medium, supplemented with 0.1% BSA. Cells were incubated for 5 h postseeding to allow network formation. Pictures of the network were taken on an inverted phase-contrast microscope (AxioObserverA; Zeiss, Jena, Germany), and network formation was assessed by counting the number of branches per field. Similar angiogenesis assays were performed to assess the effect of MP-derived paracrine factors, by adding conditioned culture media (CCMs) to HUVECs seeded onto Matrigel. In a subset of these studies, the influence of MPs-CCM on in vitro angiogenesis was assessed in the presence of high oxidative stress by adding 300 μmol/L H_2O_2 to the media. All experiments were performed in duplicate.

ELISA of MPs-CCMs

Levels of vascular endothelial growth factor vascular endothelial growth factor-A, IGF-I, MCP-1, SPARC (secreted protein, acidic, and rich in cysteine), hepatocyte growth factor, fibroblast growth factor, and angiopoietin (Ang)-2 in MPs-CCMs were measured by ELISA using Duo Set kits (R&D Systems/Bio-Techne). Levels of Ang-1 were analyzed using the Human Angiopoietin-1 ELISA Kit (Sigma-Aldrich). All analyses were performed following the manufacturer instructions in triplicate (25 μL of sample per replicate).

Studies of MP-Derived Exosomes

Exosomes were isolated by sequential ultracentrifugation from MPs-CCMs collected after 40 h of growth in a medium added with 20% exosome-free FBS, as previously described (28,29). Exosome-like microparticle abundance was revealed through nanoparticle tracking analysis, and aliquots of the same preparation were added to HUVECs in the Matrigel assay.

HUVEC Redox State

The HUVEC intracellular redox state after treatment with MPs-CCMs was investigated by using a lentiviral vector encoding for the redox-sensing green fluorescent protein (roGFP), which reports the reduced glutathione/oxidized glutathione balance (30). After overnight treatment of HUVECs with MPs-CCMs, H_2O_2 (100 and 300 μmol/L) was added. Fluorescence measurements were performed in clear 24-well plates (Corning, Lowell, MA) on a fluorescence plate reader GENios plus (Tecan, Männedorf, Switzerland) using a 535-nm emission filter. The degree of oxidation of the roGFP was estimated from the ratios of light intensities obtained during 1-min intervals under 400- and 485-nm excitation.

Reactive Oxygen Species Analysis

The production of reactive oxygen species (ROS) by MPs was evaluated by labeling cells with MitoSox (Invitrogen) according to the manufacturer instructions. Briefly, semiconfluent MPs were treated for 10 min with 5 μmol/L MitoSox dye in culture. Fluorescence was analyzed using a FACSCanto flow cytometer and the FACSDiva software (BD Biosciences). In inhibitory studies, the scavenger *N*-acetyl-cysteine (NAC; 1 mmol/L; Sigma-Aldrich) was added to MPs to infer the impact of ROS on the functions of MPs.

PKCβII Inhibition

Functional assays were performed on MPs treated with the PKCβII inhibitors LY333531 (200 nmol/L) or CGP53353 (2 μmol/L), or with vehicle. Pharmacological inhibition was extended for 7 days in the myogenic differentiation assays, and for 24 h in the proliferation and angiogenesis assays.

Gene Expression Analysis

RNA was extracted using the miRNeasy Mini Kit (Qiagen) according to the manufacturer instructions. cDNA was synthesized using the TaqMan Reverse Transcription kit and then was analyzed using the QuantStudio 6 Flex Real-Time PCR System, normalizing the data to the 18*S* rRNA. Primers for the CH2 domain of the p66 isoform were designed as follows:

5′GATCCCGAATGAGTCTCTGTCATCGTTGATATCCGCGA
TGACAGAGACTCATTCTTTTTTCCAAA-3′
and
3′GGCTTACTCAGAGACAGTAGCAACTATAGGCGCTCT
GTCTCTGAGTAAGAAAAAAGGTTTTCGA-5′.

Western Blot

Cells were harvested after overnight serum starvation in lysis buffer (TRIS-HCl 20 mmol/L, NaCl 150 mmol/L, EDTA 1 mmol/L, EGTA 1 mmol/L, Triton X-100 1%) supplemented with 1× COMPLETE protease inhibitor cocktail (Roche), 1× phosphatase inhibitor cocktail type II and III (Sigma-Aldrich), and 1× Benzonase (Novagen). Twenty-five micrograms of total cell lysates were loaded onto a NuPAGE 10% Bis-Tris precast gel (Life Technologies). Proteins were then transferred onto an Amersham Hybond polyvinylidene fluoride membrane (0.45 μm; GE Healthcare). Membranes blocked with 5% skim milk in 0.1% PBS-TWEEN 20 were decorated with mouse monoclonal primary antibodies diluted according to the manufacturer instructions. Membranes were subsequently incubated with horseradish peroxidase–conjugated anti-mouse secondary antibody (1:1,000 in 5% skim milk in 0.1% PBS-TWEEN 20). Bands were revealed using the C-Digit blot scanner (LI-COR Biosciences).

Statistical Analysis

Continuous variables were expressed as the mean ± SEM and compared using parametric tests (*t* test and ANOVA), unless not normally distributed. A P value <0.05 was considered statistically significant. The GraphPad Prism 5 software package was used for these analyses.

RESULTS

Negative Impact of Diabetes on Muscle Anatomy and Pericyte Abundance

A comparative analysis of muscle specimens from control and patients with diabetes was performed to assess the organization of myofibers and vascular cell structure. As illustrated in Fig. 1*A*, left panel, muscle sections from patients with diabetes show abundant and enlarged adipocytes (black star), and myofibers featuring degeneration (arrow) and nuclear centralization (arrowhead). Also, the average myofiber cross-section area was shifted to lower values in the diabetic samples compared with controls (Fig. 1*A*, right panel). Moreover, we observed an inflammatory infiltrate in diabetic samples, as evidenced by the abundance of $CD3^+$ lymphocytes and, particularly, $CD68^+$ macrophages (Fig. 1*B*), which is in line with findings of a previous investigation of ischemic muscles (31). Additionally, the count of $CD31^+$ capillaries revealed a significant decrease in muscle vascularization (Fig. 1*C*).

MPs embracing $CD31^+$ capillary ECs were identified by immunocytochemistry for NG2 (Fig. 1*D*) and ALP (Fig. 1*D* and Supplementary Fig. 1*A* and *B*). An unbiased profiler analysis performed using the Cell Profiler software (32) indicates a remarkable reduction in the density of ALP^+ MPs in diabetic muscles (Fig. 1*D*, bottom panel).

Diabetic MPs Show Ultrastructural Alterations but Maintain Typical Antigenic Markers

Transmission electron microscopy analyses indicate ultrastructural alterations of D-MPs, consisting of blebbing

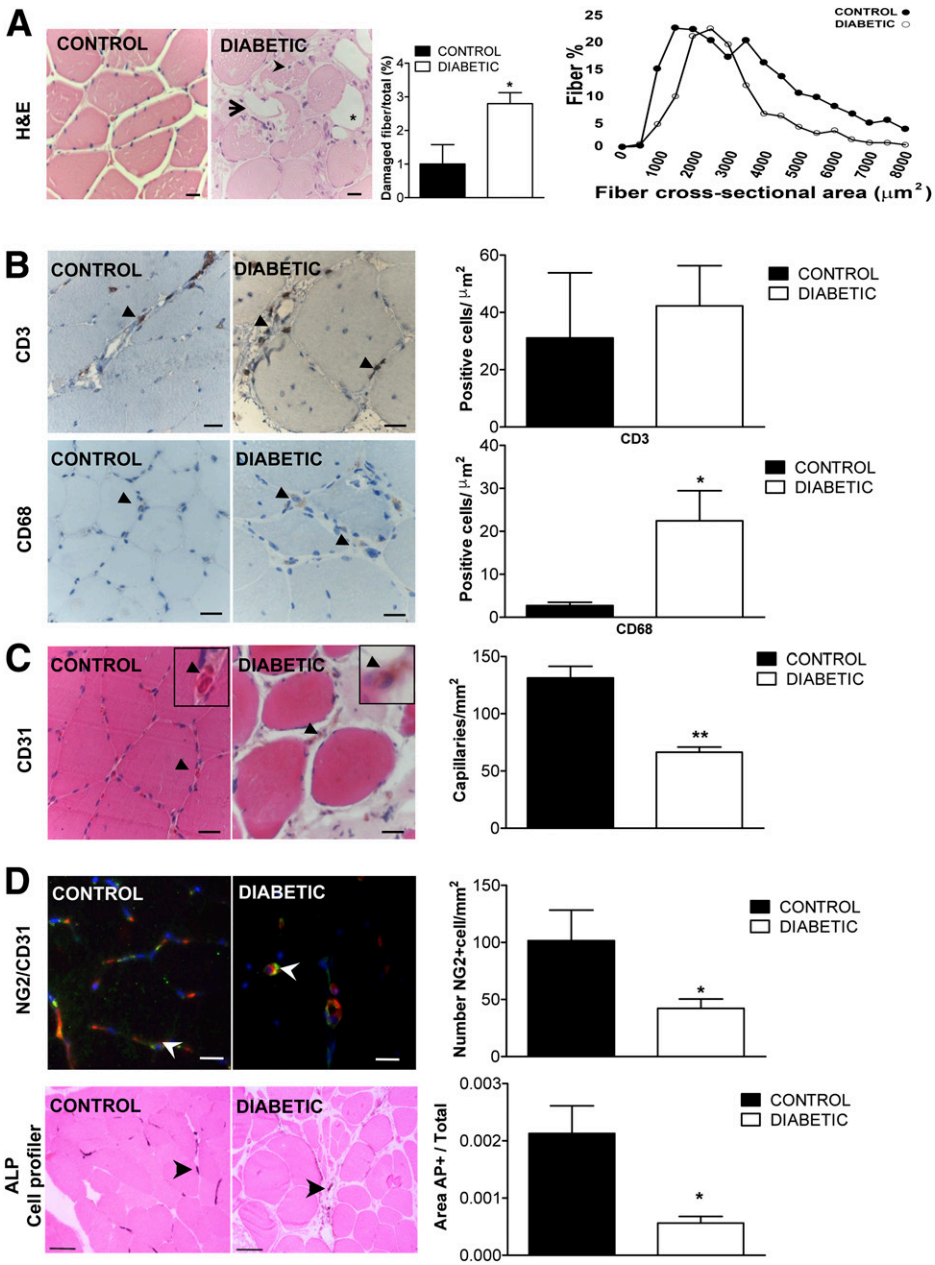

Figure 1—In situ characterization of MPs. *A*: Representative microphotographs of hematoxylin-eosin (H&E)–stained sections of human muscles. The arrow indicates degenerated fibers, whereas the arrowhead points at a centralized nucleus. Fat deposition is indicated by the black star. Quantitative analysis is depicted in the bar graph. Fiber composition was compared between C-MPs and D-MPs, measuring the cross-sectional area (left panel). Scale bars, 20 μm. *B*: The presence of inflammatory cell infiltration was quantified by immunohistochemistry using anti-CD3 and CD68 antibodies to detect, respectively, lymphocytes and macrophages (arrowheads). Macrophage infiltration was significantly increased in D-MPs. $^{*}P < 0.05$ vs. controls, $n = 4$. Scale bars, 20 μm. *C*: Capillaries in the sections are indicated by brown $CD31^{+}$ staining (black arrowheads) used for the quantification expressed in the bar graph. Values are expressed as the mean ± SEM of three control subjects and nine subjects with diabetes; $^{**}P < 0.01$ vs. controls. Scale bars, 20 μm. *D*: Within the muscle structure, pericytes, which encircle capillaries ($CD31^{+}$ cells), were identified by NG2 expression (white arrowheads). Nuclei were counterstained with DAPI. Pericyte count is shown in the bar graph. $^{*}P < 0.05$ vs. control. Scale bars, 20 μm. In addition, pericytes were identified by positivity for ALP using the Cell Profiler software. The number of ALP^{+} pericytes in muscles from patients with diabetes was significantly reduced with respect to control subjects. Black arrowheads indicate ALP-positive pericytes within the muscle section. Values expressed as the mean ± SEM on three different donors. $^{*}P < 0.05$ vs. control subjects. Scale bars, 100 μm.

and vacuolation (Fig. 2*A*). Immunocytochemistry studies confirm the pericyte identity of freshly isolated cells, based on the expression of ALP, CD146, and NG2 (Fig. 2*B* and *C*). Expanded MPs express the same markers, although they are negative for the satellite cell marker PAX7 (Fig. 2*D*). Moreover, expanded MPs coexpress NG2 and ALP (Fig. 2*E*). Flow cytometry analyses indicate the statement of mesenchymal markers CD44 and CD90

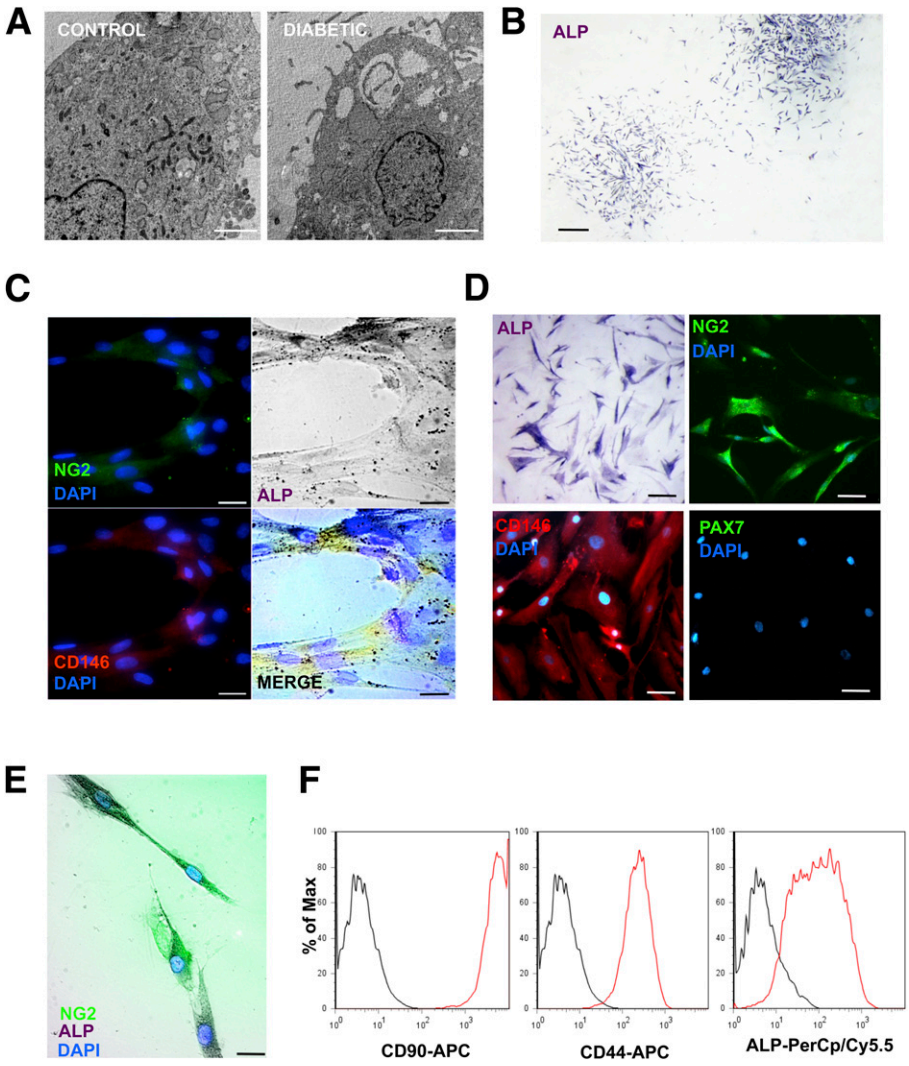

Figure 2—Characterization of isolated MPs. *A*: Transmission electron microscopy ultrastructure of MPs. Original magnification ×7,100. Scale bars, 20 μm. ALP immunostaining (*B*) and NG2 and CD146 immunofluorescence (*C*) of MPs after isolation from muscle biopsy samples. Positive cells were stained purple. Scale bars, 20 μm. *D*: MP expression of ALP, NG2, CD-146, and PAX7 to assess the antigenic characteristics of isolated cells. Nuclei were counterstained with DAPI. Scale bars, 50 μm. *E*: Double staining of MPs with ALP and anti-NG2. Scale bar, 10 μm. *F*: Flow cytometry analysis of MPs. Data are shown as peaks of positivity in reaction to staining (red line) for the markers CD90, CD44, and ALP vs. a negative control (dark line).

(Fig. 2*F*). MPs from control subjects or patients with diabetes did not differ from each other regarding antigen expression, except for desmin, which was downregulated in D-MPs (Supplementary Fig. 2*A*–*C*).

D-MPs Display Angiomyogenic Deficits

High-confluence MPs differentiate and fuse forming MyHC$^+$ syncytial myotubes (33,34). As shown in Fig. 3*A*, D-MPs have reduced capacity to generate MyHC$^+$ myotubes compared with control MPs (C-MPs), which may be ascribed in part to decreased proliferation, resulting in delayed cell confluence (Fig. 3*B*). Additionally, we found that D-MPs have an increased propensity to differentiate into adipocytes (1.7 ± 0.8-fold increase compared with C-MPs, $n = 3$; Supplementary Fig. 2*D*). In contrast, diabetes did not affect apoptosis, as assessed by caspase activity (6.7 ± 2.2 vs. 7.3 ± 2.4 relative fluorescence units at 499 and 521 nm in control subjects) or cell motility in a scratch assay at both 5 h postscratch (8.7 ± 3.7% vs. 3.6 ± 1.7% wound closure in control subjects) and 24 h postscratch (60.0 ± 13.8 vs. 43.4 ± 17.4% in control subjects).

We next analyzed the ability of MPs to form networks on Matrigel. Both C-MPs and D-MPs were able to form branched structures. In comparison with networks formed by HUVECs, the MP structures consisted of longer tubes and wider meshwork (Fig. 3*C*). When cocultured with HUVECs, MPs locate near the intersection points or around the endothelial tubes (Fig. 3*D*, white arrow and arrowhead). Importantly, D-MPs have detrimental effects on network formation, resulting in a less reticulated system (Fig. 3*E*).

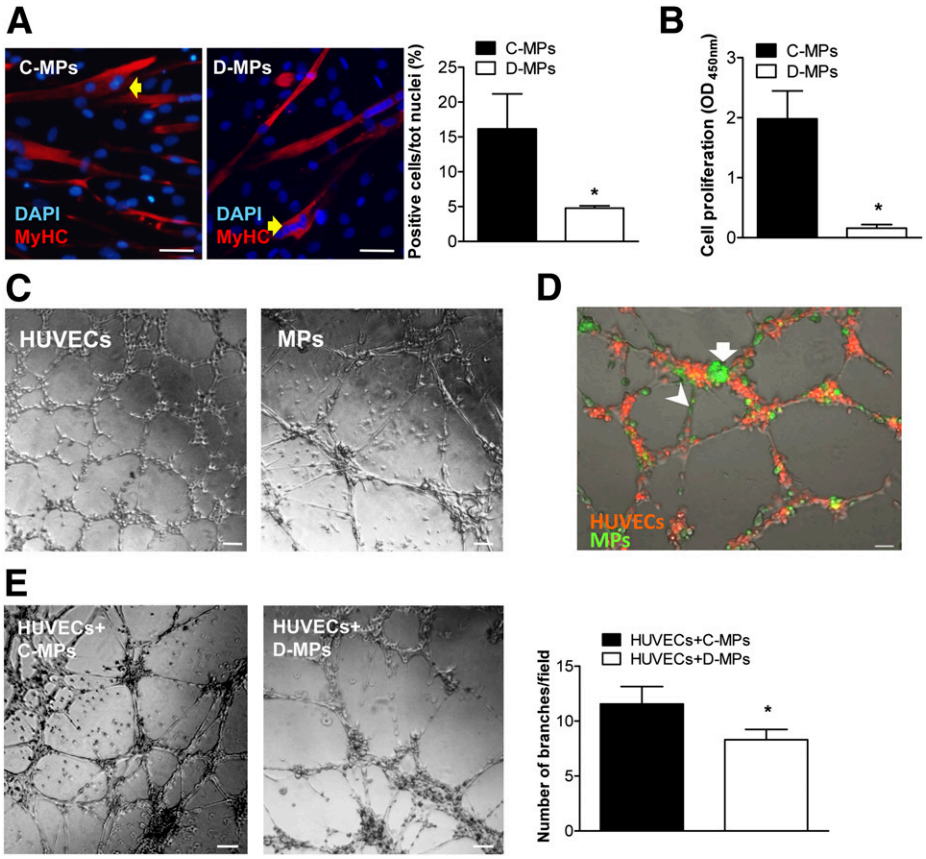

Figure 3—MP differentiation, proliferation, and network formation. *A*: Muscle differentiation: MPs were stained with anti-MyHC antibody to reveal syncytial myofiber-like structures (yellow arrowheads) generated by fusion. Nuclei were counterstained with DAPI. The bar graph summarizes the number of MyHC$^+$ fibers counted on the total number of nuclei per field. Counts were made on five pictures from at least three biological replicates. Original magnification ×20. Scale bars, 50 μm. Values are expressed as the mean ± SEM. *$P < 0.05$ vs. C-MPs. *B*: Cell proliferation was measured as optical density (OD) after 48 h of culture, of which the last 24 h occurred in the presence of BrdU, as described in RESEARCH DESIGN AND METHODS. Values are expressed as the mean ± SEM of four experiments in triplicate. *$P < 0.05$ vs. C-MPs. *C*: Matrigel assay: compared with HUVECs (left panel), MPs (right panel) form networks that are less reticulated with thicker nodes and longer tubes. Scale bars, 100 μm. *D*: HUVEC-MP interaction on Matrigel. Fluorescent microphotograph of networks formed on Matrigel by coculturing HUVECs (stained red with PKH26 dye) and MPs (stained green with PKH67 dye) at ×5 magnification. MPs locate preferentially at nodes of the network (white arrow). They are also located along the tube assisting HUVECs in tubulization (white arrowhead). Scale bar, 100 μm. *E*: Direct interaction with ECs (HUVECs): microphotographs of networks formed by MPs in coculture with HUVECs at a 1:4 MP/HUVEC ratio. Bar graphs represent the efficiency of network formation in terms of the number of branches. Values are expressed as the mean ± SEM of at least five experiments in duplicate; *$P < 0.05$ vs. HUVECs+C-MPs. Scale bars, 100 μm.

Paracrine Deficits of D-MPs

To investigate whether paracrine mechanisms are responsible for the negative impact of D-MPs on angiogenesis, we next tested the effect of MP-CCM on HUVECs in the Matrigel assay. As shown in Fig. 4*A*, the D-MP-CCM induces a decrease in network formation, suggesting an alteration of the secretome. To verify this possibility, we interrogated secreted angiogenic myokines. ELISA showed significantly decreased levels of proangiogenic factors (i.e., vascular endothelial growth factor-A, IGF-I, and Ang-1, in D-MP-CCM (Fig. 4*B*).

Specific micro-RNAs (miRs) have recently been shown to regulate angiogenesis, and their deregulation may contribute to vascular complications and ischemia (29,35–37). Data from PCR analysis did not show any difference between D-MPs and C-MPs in the expression of classic angio-miRs, miR-16, miR-503, and miR-27b (Supplementary Fig. 3*A*). Also, the analysis of CCMs confirmed that D-MPs and C-MPs secrete similar amounts of miR-16, whereas miR-503 and miR-27b were undetectable (data not shown). Likewise, no difference was observed in the expression of the miR-27b targets thrombospondin-1, sprouty-2, and semaphorin 6A (Supplementary Fig. 3*Aii* and *B*), which are negative modulators of angiogenesis (36).

Secreted exosomes mediate the functional cross-talk between pericytes and ECs (29,37,38). Therefore, we next investigated whether diabetes has an impact on the capacity of MPs to release exosomes or modifies exosome activity upon angiogenesis. Results indicate no difference in exosome-sized vesicles shed by C-MPs and D-MPs ($7.4 \pm 2.5 \times 10^{-4}$ vs. $6.9 \pm 2 \times 10^{-4}$ exosome concentration/cell, respectively). Also, the addition of exosomes

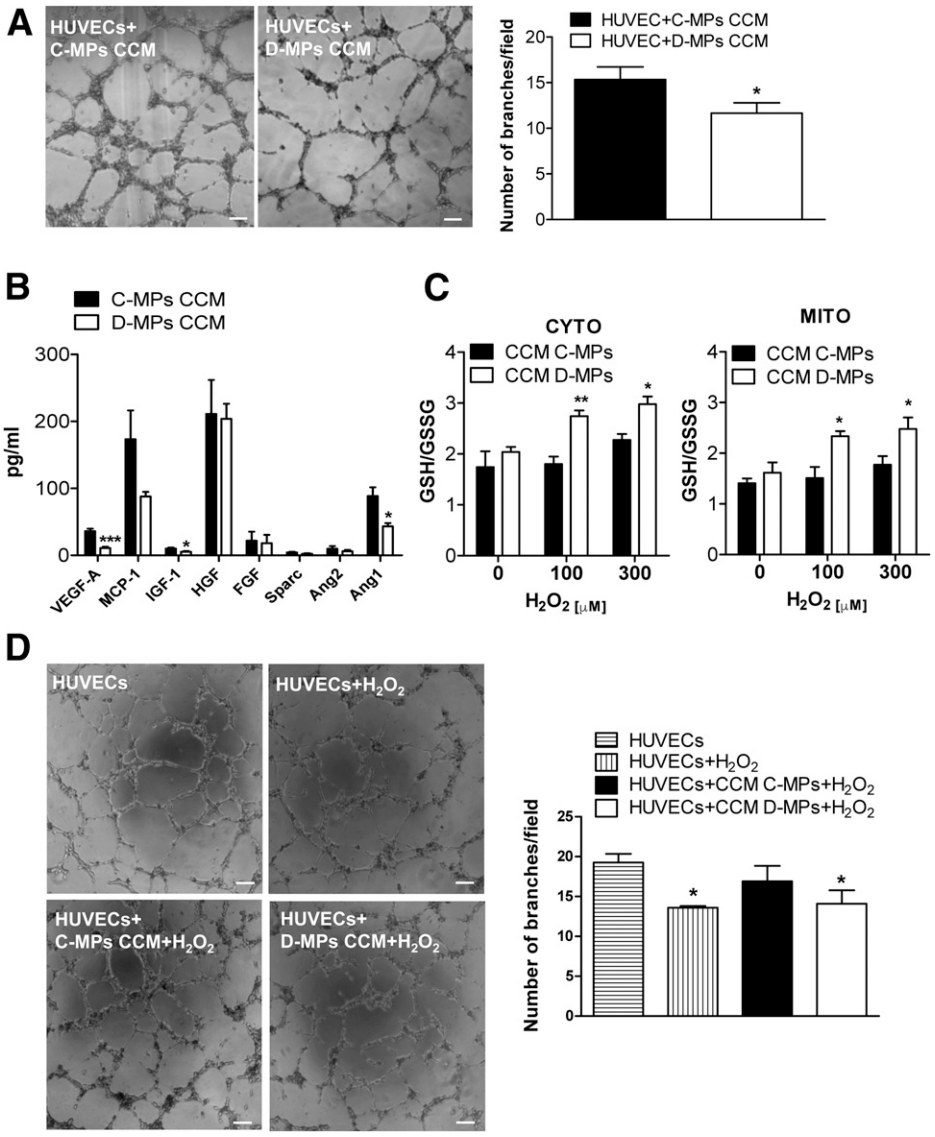

Figure 4—Paracrine effect of MPs on HUVECs. *A*: Matrigel assay performed with HUVECs at 5×10^4 cell density in the presence of MP-CCM. Bar graphs represent the efficiency of network formation (number of branches). Values are expressed as the mean ± SEM of five experiments in duplicates. $^*P < 0.05$ vs. HUVECs+C-MPs-CCM. Scale bars, 100 μm. *B*: Myokines regulating angiogenesis were analyzed by ELISA in MPs-CCM. $^*P < 0.05$ vs. C-MPs; $^{***}P < 0.001$ vs. C-MPs in at least 3 samples. Data are represented as the average of each condition (control vs. diabetic) with a standard error of the mean. *C*: roGFP-expressing HUVECs were used as a tool to analyze the HUVEC susceptibility to oxidative stress. Values expressed as mean fluorescence ± SEM of 3 experiments in quadruplicates. $^*P < 0.05$ and $^{**}P < 0.01$ vs. C-MPs-CCM. *D*: HUVECs were treated during network formation with 300 μmol/L H_2O_2 to test the effect of oxidative stress. MPs-CCM were also supplemented with 300 μmol/L H_2O_2 and added to HUVECs. Network formation was quantified as number of branches. Values expressed as mean ± SEM of four experiments in duplicate. $^*P < 0.05$ vs. HUVECs. Scale bars, 100 μm. CYTO, cytosolic; GSH, glutathione; GSSG, oxidized glutathione; MITO, mitochondrial.

from D-MPs to HUVECs in a Matrigel assay does not alter the network formation (10.7 ± 1.9 vs. 10.8 ± 0.4 intersections/field in HUVECs plus C-MPs), although exosome-depleted D-MP-CCM still inhibits the process (data not shown).

We next investigated the role of ROS as paracrine mediators of the negative cross-talk between D-MPs and ECs. To this end, HUVECs were transduced with lentiviral vectors carrying the cytosolic or the mitochondrial isoforms of roGFP, which act as fluorescent indicators of the intracellular redox status (30), and were then incubated with C-MP-CCM or D-MP-CCM before being exposed to increasing doses of the pro-oxidant H_2O_2. We found that C-MP-CCM protects HUVECs from the pro-oxidant action of H_2O_2, whereas D-MP-CCM does not (Fig. 4*C*). In additional experiments, we test whether ROS per se impairs angiogenesis in vitro. To this end, HUVECs were exposed to a fixed dose of H_2O_2 (300 μmol/L) before being seeded into the Matrigel assay. As expected, H_2O_2 inhibited the HUVEC network formation capacity in a

way that was comparable to the inhibition caused by D-MPs or their CCM. Interestingly, the addition of C-MP-CCM contrasted the inhibitory effect of H_2O_2 on network formation, whereas the D-MP-CCM were ineffective (Fig. 4*D*).

ROS Blockade Reverts Functional Deficits of D-MPs

We next investigated the redox status of C-MPs and D-MPs by staining cells with MitoSox, a dye that selectively reacts with superoxide anion $O_2^{\cdot}$ in mitochondria. The results of flow cytometry analyses indicate that D-MPs have remarkably increased oxidative stress levels compared with C-MPs, considering either the average MitoSox dye intensity or the number of MitoSox$^+$ cells (Fig. 5*A*). Moreover, the ROS scavenger system involved in the maintenance of cellular redox balance was depressed, as indicated by the downregulation of SOD-1 and catalase (Fig. 5*B*). To confirm that the ROS imbalance contributes to the dysfunction of D-MPs, we investigated whether the addition of NAC, a generic antioxidant, restores inherent and paracrine activities of the diabetic cells. In line, NAC partially amended the myogenic differentiation capacity of D-MPs (Fig. 6*A*), restored the proliferation of D-MPs (Fig. 6*B*), and abrogated the inhibitory effect of D-MP-CCM on HUVEC network formation in vitro (Fig. 6*C*). Since the excess of ROS activates the p66^{Shc} signaling pathway by its selective phosphorylation, the next step was to compare the levels and phosphorylation state of this protein in C-MPs and D-MPs.

Implication of p66^{Shc} in the Redox Imbalance of D-MPs

Using primers specifically designed for the p66 isoform of Shc1 protein, we found that p66^{Shc} mRNA expression is significantly upregulated in D-MPs compared with C-MPs (Fig. 7*A*). Under unbalanced redox conditions, p66^{Shc} is phosphorylated at the Ser36 of its unique CH2 domain and translocates to the mitochondrial transmembrane space, where it fuels additional ROS production, causing the formation of a permeability-transition pore and apoptosis. We analyzed the phosphorylation state of p66^{Shc} in MPs by different methods. Using a specific Western blot Ser36-p-p66^{Shc} antibody, we observed an increase in the band of activated p66^{Shc} with no difference in the total protein content (Fig. 7*B*). Flow cytometry (Fig. 7*C*) and immunocytochemistry (Fig. 7*D*) confirmed the increased statement of phospho-p66^{Shc} in D-MPs. Nonetheless, treatment of D-MPs with NAC was ineffective in restoring p66^{Shc} phosphorylation to control levels (Supplementary Fig. 4*A* and *B*). This result has different keys of interpretation. First, the thiol groups of the NAC molecule may undergo auto-oxidation processes, especially in culture, which reduces their activity. Thus, a possible explanation is that NAC did not reach biologically relevant concentrations in mitochondria, where active p66^{Shc} accumulates. Alternatively, p66^{Shc} activation by PKCβII may be partially independent of ROS or resistant to temporary ROS reduction. The latter possibility is compatible with a reported epigenetic activation of the p66^{Shc} promoter in the context of diabetes (39). Also, ROS scavenging by NAC may be insufficient to contrast the activity of

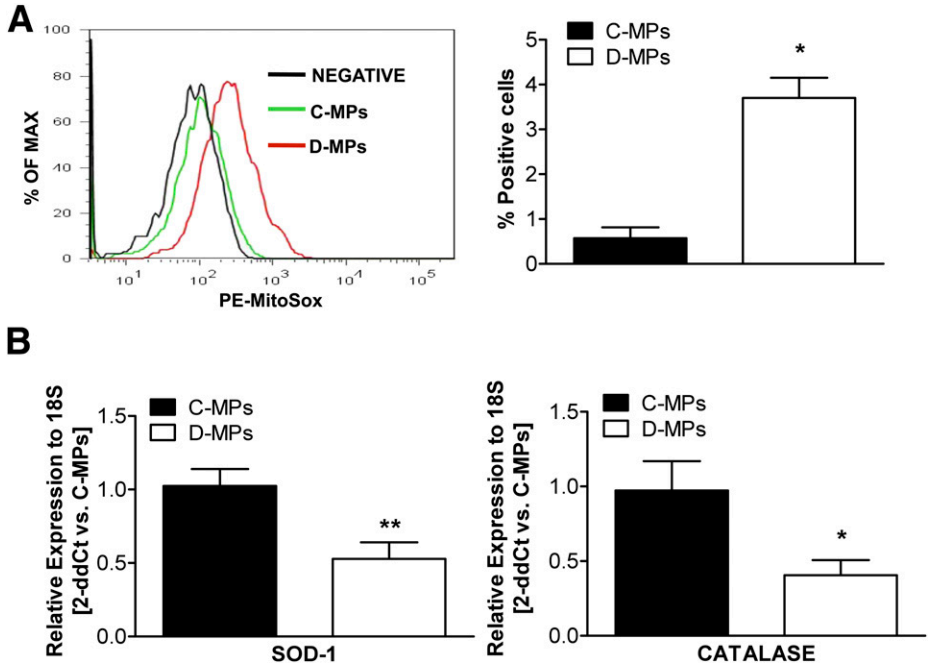

Figure 5—Analysis of pericyte redox status. *A*: MPs were stained with 5 μmol/L MitoSox and read on a FACSCanto II flow cytometer in the PE channel. Data are quantified in the bar graph. Values are expressed as the mean ± SEM of percentages of positive populations. Sample size $n = 4$. *$P < 0.05$ vs. C-MPs. *B*: Transcriptional analysis of the antioxidant genes SOD-1 and catalase. Values are expressed as the mean ± SEM of five experiments. *$P < 0.05$ vs. C-MPs; **$P < 0.01$. PE, phycoerythrin.

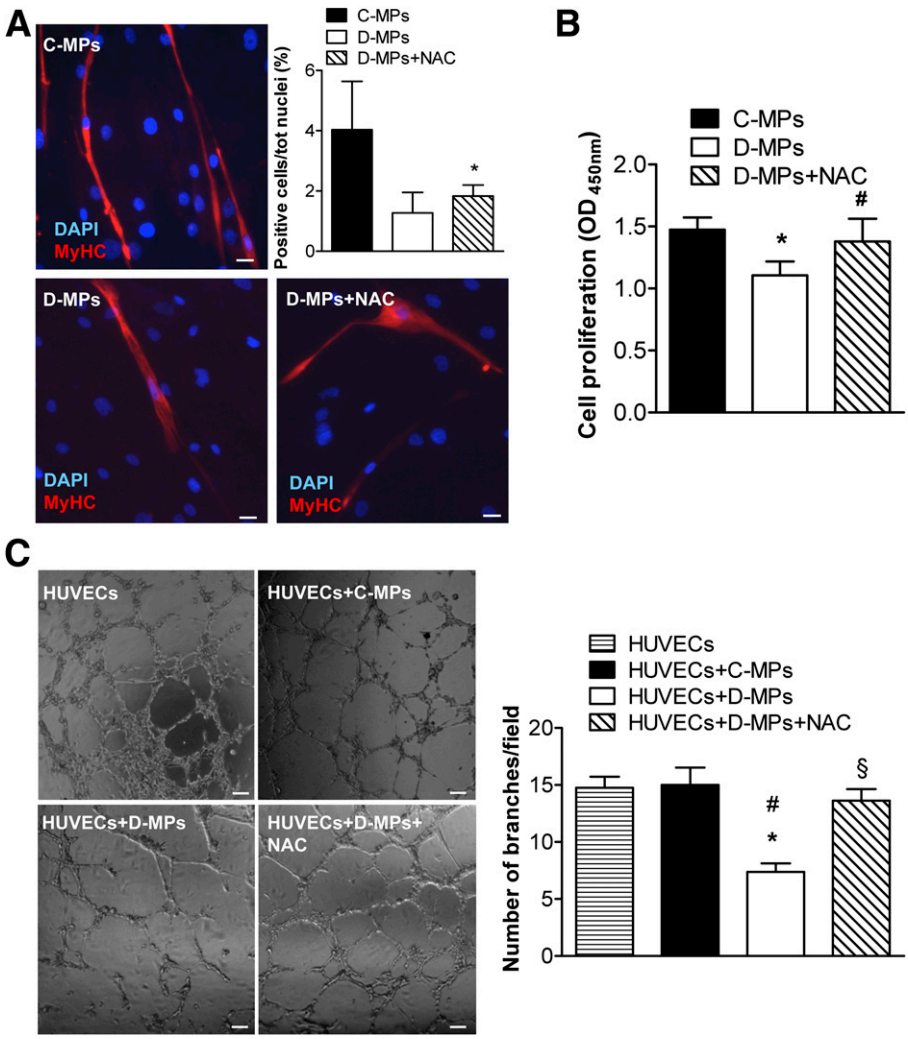

Figure 6—NAC restores D-MP functions. *A*: Myotube differentiation was evaluated by assessing MyHC-expressing cells. Quantification was performed by counting the number of MyHC-expressing cells on the total cells, which are expressed here as bar graphs. **P* < 0.05 vs. D-MPs in at least four samples. Scale bars, 50 μm. *B*: Cell proliferation measured by BrdU incorporation assay after 30-min exposure to NAC (1 mmol/L) prior to the addition of BrdU. Values are expressed as the mean ± SEM of four experiments performed in triplicate per group. **P* < 0.05 vs. C-MPs; #*P* < 0.05 vs. D-MPs. *C*: Matrigel-assisted HUVEC network formation was analyzed after D-MPs treatment with NAC (1 mmol/L for 30 min). Representative microphotographs and bar graphs show the efficiency of network formation as assessed by counting the number of branches. Values are expressed as the mean ± SEM of three experiments performed in duplicate. **P* < 0.05 vs. HUVECs; #*P* < 0.05 vs. HUVECs+C-MPs; §*P* < 0.05 vs. HUVECs+D-MPs. Scale bars, 100 μm. OD, optical density.

protein kinases responsible for $p66^{Shc}$ phosphorylation, namely PKCβII (40). Accordingly, we found that NAC supplementation does not affect PKCβII localization or expression (Supplementary Fig. 4*C* and *D*).

Suppression of $p66^{Shc}$ Activity by PKCβII Inhibition Reverts Functional Deficits of D-MPs

To assess the direct involvement of $p66^{Shc}$ in the dysfunction of D-MPs, $p66^{Shc}$ activation was blocked by interfering with its phosphorylation. To this purpose, we inhibited the PKCβII kinase, which is responsible for $p66^{Shc}$ activation (39). Two compounds were used to inhibit PKCβII in D-MPs: LY333531, also known as Ruboxistaurin, which has already been tested for therapeutic efficacy in clinical trials of diabetic retinopathy, and CGP53353 (41). Flow cytometry confirmed that both LY333531 and CGP53353 reduce the levels of Ser36-phospho-$p66^{Shc}$ (Fig. 8*A*). We next reassessed the features of the dysfunction of D-MPs after treatment with PKCβII inhibitors. Results indicate an overall functional improvement upon PKCβII inhibition, including myogenic differentiation (Fig. 8*B*), proliferation (Fig. 8*C*), and interference with network formation (Fig. 8*D*) Those data indicate that blocking the PKCβII-$p66^{Shc}$ pathway may have important therapeutic implications for total restoration of the functions of D-MPs.

DISCUSSION

The current study is the first to investigate the anatomical, functional, and molecular diversity of MPs from

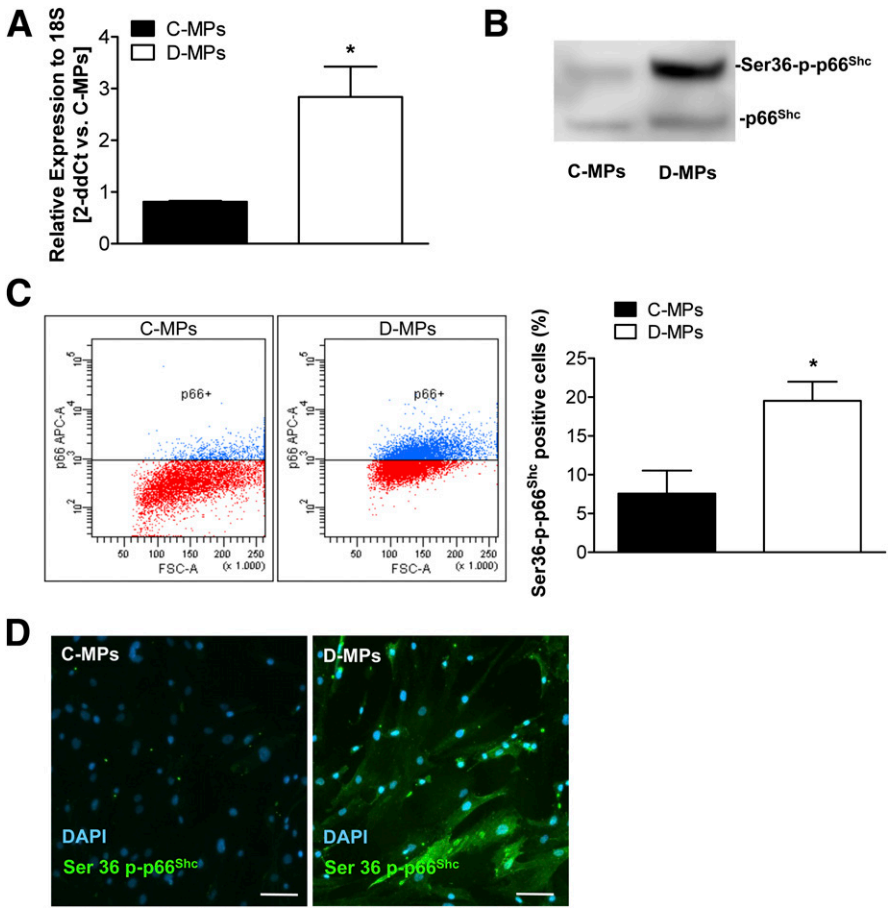

Figure 7—Induced p66^{Shc} expression in D-MPs. *A*: Transcriptional analysis of the ROS sensor protein p66^{Shc}. Values are expressed as the mean ± SEM of three experiments. *P < 0.05 C-MPs. *B*: Western blot: C-MPs (lane 1) and D-MPs (lane 2) were compared for the expression of both total p66^{Shc} and serine phosphorylated (Ser36-p-p66^{Shc}) isoforms using the anti-Ser36-p-p66^{Shc} clone 6E10. *C*: Flow cytometry analysis and quantification of the percentage of Ser36-p-p66^{Shc+} cells are expressed as the mean ± SEM of three experiments. *P < 0.05 vs. C-MPs. *D*: Immunofluorescence microscopy analysis of phospho-p66^{Shc+} MPs. Scale bars, 50 μm.

skeletal muscles of patients with diabetes who have CLI. Importantly, MPs were isolated from the tissue immediately at the rim of normal tissue surrounding the plane of dissection, a critical zone where it is mandatory to concentrate efforts for limb salvage. Results show for the first time specific alterations consisting of ultrastructural modifications, proliferative impairment leading to blunted myogenic potential, and acquisition of an anti-angiogenic activity. Altogether, these deficits could contribute to the extension and severity of peripheral complications. Importantly, we discovered that the diabetes-associated incompetence of MPs is attributable to increased ROS levels, weakened antioxidative protection, and an activated PKCβII-p66^{Shc} signaling pathway. Also, excessive ROS production and release transmit negative signals to adjacent vascular cells. Muscle regeneration via trans-differentiation of MPs and satellite cells into myoblasts is crucial for the recovery of damaged muscles, whereas the overgrowth of adipogenic cells may be deleterious. Some studies (42) suggest that a subset of MPs contribute to fat accumulation. Our investigation shows structural data that are compatible with a differentiation bias of MPs favoring adipogenesis at the detriment of myogenesis. Concurrent mechanisms may participate in this adverse remodeling, including poor metabolic control, ischemia, and lack of exercise (43).

Unraveling the molecular mechanisms underpinning the dysfunction of MPs could help develop new strategies to maintain tissue integrity and improve clinical outcomes, especially after major limb amputation, a condition associated with high mortality. Current mechanistic understanding of diabetic vasculopathy is mainly inferred from animal models (44). However, the clinical transferability of data from rodents mimicking human diabetes/CLI is limited and often equivocal. Therefore, the successful isolation of MPs from the muscles of patients with diabetes undergoing major limb amputation for CLI discloses excellent opportunities for disease modeling and therapeutics. Since there is a potential overlapping between MPs and satellite cells, it was essential to ascertain that isolated cells express high levels of the canonical pericyte marker NG2 and ALP, along with mesenchymal

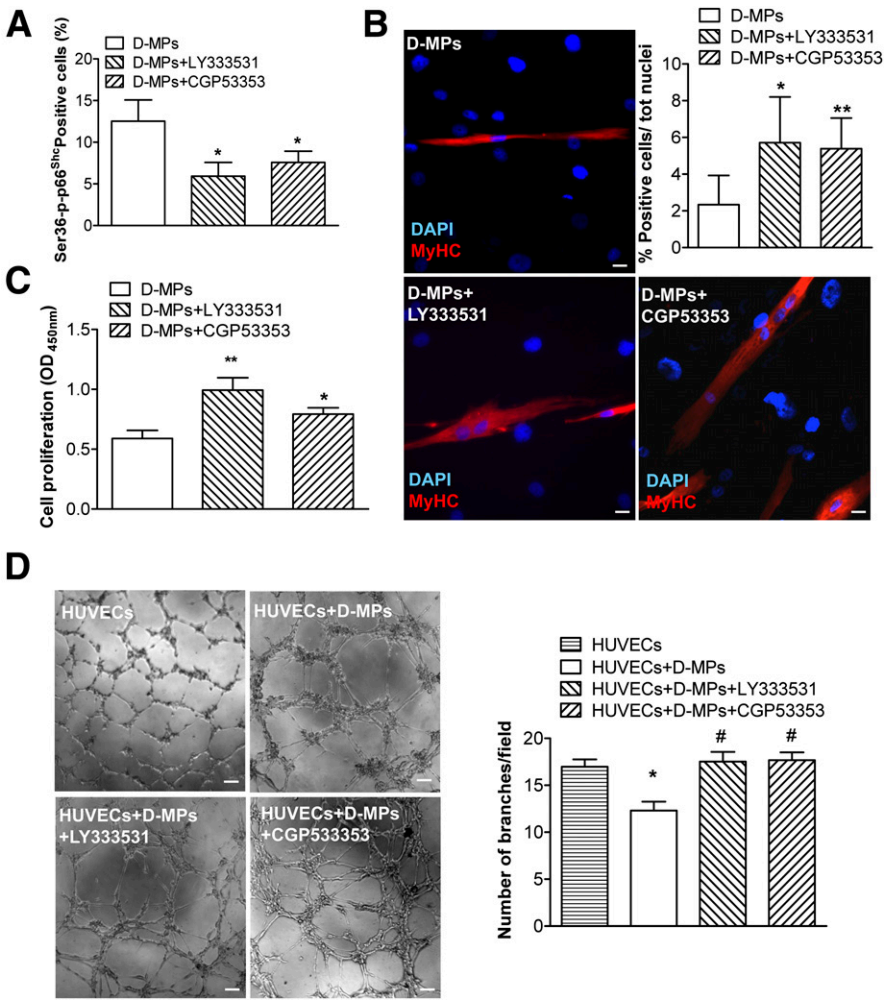

Figure 8—PKCβII inhibitors LY333531 and CGP53353 restore the functions of D-MPs, counteracting $p66^{Shc}$ activation. *A*: The selective inhibition of kinase PKCβII responsible for the phosphorylation-mediated activation of $p66^{Shc}$ was achieved treating D-MPs with 200 nmol/L LY333531 or 2 μmol/L CGP53353. Cell functions like myogenic differentiation (*B*), proliferation (*C*), and network formation on Matrigel (*D*) were all recovered after PKCβII inhibition–dependent $p66^{Shc}$ blockade. Values are expressed as the mean ± SEM. **P* < 0.05 vs. D-MPs; ***P* < 0.01 vs. D-MPs. For Matrigel assay **P* < 0.05 vs. HUVECs; #*P* < 0.05 vs. HUVEC+D-MPs (*n* = 3). Scale bars, 50 μm for myogenic differentiation pictures (original magnification ×20) and 100 μm for Matrigel microphotographs (original magnification ×25). Sample size *n* = 4. OD, optical density; tot, total.

markers (CD90 and CD44), and the staminal marker CD146, although being negative for PAX7. In fact, ALP positivity and PAX7 negativity are determinants to distinguish pericytes from $ALP^{-}/PAX7^{-}$ mature myocytes or $ALP^{-}/PAX7^{+}$ satellite cells. When grown to overconfluence, MPs spontaneously fuse together to form syncytial myotubes expressing MyHC. Interestingly, the ability to form syncytial myotubes was drastically reduced in D-MPs, and this could be one of the reasons (together with satellite cell dysfunction) of the aberrant tissue repair of diabetic skeletal muscles.

Skeletal muscle physiology is maintained by mutual trophic influences among MPs, ECs, and myocytes (45). However, this cross-talk is perversely modified by diabetes. The present investigation integrates the results of our recent study showing that p75NTR expression in ECs exposed to high glucose activates the transcription of miR-503, which negatively affects pericyte function (37,46). Here, we newly show that D-MPs exert a drastic reduction of the ability of ECs to form in vitro networks through an alteration in the secretion of angiogenic growth factors. Instead, the screening of several classic angio-miRs or exosomes did not provide any supplementary clue.

An additionally accountable mechanism emerged from studies of the MP redox state and was confirmed by the recognition of a reduced scavenging capacity of D-MPs, consisting of the downregulation of SOD-1 and catalase gene expression. Accordingly, the restoration of the physiological redox state by NAC supplementation led to the correction or attenuation of D-MP dysfunctions. A more in-depth analysis of the original culprit directed us to recognize the intracellular stress sensor as $p66^{Shc}$ protein. Several lines of evidence support this possibility, as follows: *1*) $p66^{Shc}$ is upregulated at the mRNA level, and

2) was hyperphosphorylated at the Ser36 residue, which corresponds to an activated pro-oxidant state of $p66^{Shc}$. However, NAC administration did not revert $p66^{Shc}$ activation so other targets are needed to suppress $p66^{Shc}$ activation. Previous studies in animal models used the abrogation or silencing of $p66^{Shc}$ to infer its pathophysiological importance. However, this approach has translational limitations because $p66^{Shc}$ is thought to have bivalent actions (47). Thus, its total suppression may not be therapeutically desirable. Therefore, we decided to interfere with the excessive phosphorylation of $p66^{Shc}$ by inhibiting PKCβII (39,41). Importantly, the use of PKCβII-specific inhibitors, namely LY333531 or CGP53353, reverted $p66^{Shc}$ phosphorylation and restored D-MP functions. Although NAC has been efficiently used to inhibit PKCβII expression in other experimental settings, dosages and cell type specificity may explain the observed differences (48,49). Moreover, NAC is susceptible to auto-oxidation in culture conditions, reducing its effectiveness. Importantly, PKCβII inhibitors lead, at least in vitro, to a more effective rescue of D-MP myogenic differentiation capacity compared with NAC treatment, thus warranting additional investigation in patients with limb ischemia. This may be clinically relevant since generic antioxidant therapy has given disappointing results in trials assessing vitamins supplementation efficacy for cardiovascular diseases (50).

In conclusion, we demonstrate that *1*) MPs can be efficiently isolated from skeletal muscles of patients without diabetes and patients with diabetes; *2*) D-MPs are dysfunctional in terms of reduced myogenic ability, decreased proliferation, and antiangiogenic properties; *3*) those alterations are strictly related to an increased oxidative status driven by $p66^{Shc}$ overexpression and activation; and *4*) antioxidant treatment as well as $p66^{Shc}$ phosphorylation blockade by inhibition of PKCβII can rescue D-MP functional competence.

These results are important since one of the used PKCβII inhibitors, LY333531, is currently at the final step of clinical trial investigation (phase 3) in patients with diabetic retinopathy. This opens invaluable opportunities for the treatment of life-threatening complications of diabetes. We hypothesize that the use of PKCβII inhibitors may halt the progression of CLI and allow surgeons to decide to perform less extensive amputations, when these become necessary, ultimately improving the quality and duration of life of patients with complicated diabetes.

Acknowledgments. The authors thank Dr. Laura Cantone from EPIGET (Epidemiologia, Epigenetica e Tossicologia) Laboratory, Dipartimento di Scienze Cliniche e di Comunità Università degli Studi di Milano, Milan, Italy, for nanoparticle tracking analysis of exosomes and the Centre of Advanced Microscopy "P. Albertano," in the Department of Biology, University of Rome Tor Vergata, for confocal images.

Funding. This work has been supported by British Heart Foundation grants RJ5905 and RM/13/2/30158 and Italian Ministry of Health grant RF-2011-02346867 to P.M., Cariplo Foundation grant 2013-0887 to G.S., European Research Council grant N322749 DEPTH to G.C., and Uncovering Excellence Grant 2014 MDESMPLAT to C.G.

Duality of Interest. No potential conflicts of interest relevant to this article were reported.

Author Contributions. R.V. participated in the study design, researched and interpreted the data, and wrote the manuscript. C.F. and E.S. isolated and characterized human pericytes. S.T. and D.M. performed immunofluorescence and histochemistry analysis. S.P. set and performed Cell Profiler analysis for ALP staining area quantification and statistical analysis. D.F.M. performed measurements of secreted factors by ELISA. G.P. and R.G. performed redox analyses of endothelial cells. G.F. and F.S. conducted and analyzed the electron microscopy studies. R.C., A.G., and S.L. are responsible for patient enrollment and muscle sample collection. G.C. and S.C. helped with the study design, data analysis interpretation, and writing of the manuscript. R.R. and C.B. helped with data interpretation. G.S., C.G., and P.M. designed the study, helped with data analysis and interpretation, and wrote the manuscript. G.S., C.G., and P.M. are the guarantors of this work and, as such, had full access to all the data in the study and take responsibility for the integrity of the data and the accuracy of the data analysis.

Prior Presentation. Parts of this study were presented in abstract form at the American Heart Association Arteriosclerosis, Thrombosis and Vascular Biology Scientific Sessions, Orlando, FL, 7–11 November 2015; at European Society of Cardiology Congress 2015, London, U.K., 29 August–2 September 2015; and at the 2015 Joint Meeting of the European Society for Microcirculation and European Vascular Biology Organisation, Pisa, Italy, 3–6 June 2015.

References

1. Selvin E, Erlinger TP. Prevalence of and risk factors for peripheral arterial disease in the United States: results from the National Health and Nutrition Examination Survey, 1999-2000. Circulation 2004;110:738–743

2. Nehler MR, Duval S, Diao L, et al. Epidemiology of peripheral arterial disease and critical limb ischemia in an insured national population. J Vasc Surg 2014;60:686–695.e2

3. Faglia E, Clerici G, Clerissi J, et al. Long-term prognosis of diabetic patients with critical limb ischemia: a population-based cohort study. Diabetes Care 2009; 32:822–827

4. Fadini GP, Boscaro E, de Kreutzenberg S, et al. Time course and mechanisms of circulating progenitor cell reduction in the natural history of type 2 diabetes. Diabetes Care 2010;33:1097–1102

5. Sen CK, Gordillo GM, Roy S, et al. Human skin wounds: a major and snowballing threat to public health and the economy. Wound Repair Regen 2009; 17:763–771

6. Relaix F, Zammit PS. Satellite cells are essential for skeletal muscle regeneration: the cell on the edge returns centre stage. Development 2012;139: 2845–2856

7. D'Souza DM, Al-Sajee D, Hawke TJ. Diabetic myopathy: impact of diabetes mellitus on skeletal muscle progenitor cells. Front Physiol 2013;4:379

8. Broholm C, Brandt C, Schultz NS, Nielsen AR, Pedersen BK, Scheele C. Deficient leukemia inhibitory factor signaling in muscle precursor cells from patients with type 2 diabetes. Am J Physiol Endocrinol Metab 2012;303:E283–E292

9. Gaster M, Rustan AC, Aas V, Beck-Nielsen H. Reduced lipid oxidation in skeletal muscle from type 2 diabetic subjects may be of genetic origin: evidence from cultured myotubes. Diabetes 2004;53:542–548

10. Scarda A, Franzin C, Milan G, et al. Increased adipogenic conversion of muscle satellite cells in obese Zucker rats. Int J Obes 2010;34:1319–1327

11. Birbrair A, Zhang T, Wang Z-M, et al. Skeletal muscle pericyte subtypes differ in their differentiation potential. Stem Cell Res (Amst) 2013;10:67–84

12. Fuoco C, Sangalli E, Vono R, et al. 3D hydrogel environment rejuvenates aged pericytes for skeletal muscle tissue engineering. Front Physiol 2014;5:203

13. Zheng B, Chen CW, Li G, et al. Isolation of myogenic stem cells from cultures of cryopreserved human skeletal muscle. Cell Transplant 2012;21:1087–1093

14. Campagnolo P, Cesselli D, Al Haj Zen A, et al. Human adult vena saphena contains perivascular progenitor cells endowed with clonogenic and proangiogenic potential. Circulation 2010;121:1735–1745
15. Gubernator M, Slater SC, Spencer HL, et al. Epigenetic profile of human adventitial progenitor cells correlates with therapeutic outcomes in a mouse model of limb ischemia. Arterioscler Thromb Vasc Biol 2015;35:675–688
16. Katare R, Riu F, Mitchell K, et al. Transplantation of human pericyte progenitor cells improves the repair of infarcted heart through activation of an angiogenic program involving micro-RNA-132. Circ Res 2011;109:894–906
17. Avolio E, Caputo M, Madeddu P. Stem cell therapy and tissue engineering for correction of congenital heart disease. Front Cell Dev Biol 2015;3:39
18. Paneni F, Costantino S, Volpe M, Lüscher TF, Cosentino F. Epigenetic signatures and vascular risk in type 2 diabetes: a clinical perspective. Atherosclerosis 2013;230:191–197
19. Giorgio M, Migliaccio E, Orsini F, et al. Electron transfer between cytochrome c and p66Shc generates reactive oxygen species that trigger mitochondrial apoptosis. Cell 2005;122:221–233
20. Pinton P, Rimessi A, Marchi S, et al. Protein kinase C beta and prolyl isomerase 1 regulate mitochondrial effects of the life-span determinant p66Shc. Science 2007;315:659–663
21. Graiani G, Lagrasta C, Migliaccio E, et al. Genetic deletion of the p66Shc adaptor protein protects from angiotensin II-induced myocardial damage. Hypertension 2005;46:433–440
22. Zaccagnini G, Martelli F, Magenta A, et al. p66(ShcA) and oxidative stress modulate myogenic differentiation and skeletal muscle regeneration after hind limb ischemia. J Biol Chem 2007;282:31453–31459
23. Natalicchio A, Tortosa F, Labarbuta R, et al. The p66(Shc) redox adaptor protein is induced by saturated fatty acids and mediates lipotoxicity-induced apoptosis in pancreatic beta cells. Diabetologia 2015;58:1260–1271
24. Geraldes P, King GL. Activation of protein kinase C isoforms and its impact on diabetic complications. Circ Res 2010;106:1319–1331
25. Danis RP, Sheetz MJ. Ruboxistaurin: PKC-beta inhibition for complications of diabetes. Expert Opin Pharmacother 2009;10:2913–2925
26. Budhiraja S, Singh J. Protein kinase C beta inhibitors: a new therapeutic target for diabetic nephropathy and vascular complications. Fundam Clin Pharmacol 2008;22:231–240
27. Sacchetti B, Funari A, Michienzi S, et al. Self-renewing osteoprogenitors in bone marrow sinusoids can organize a hematopoietic microenvironment. Cell 2007;131:324–336
28. Théry C, Amigorena S, Raposo G, Clayton A. Isolation and characterization of exosomes from cell culture supernatants and biological fluids. Curr Protoc Cell Biol 2006;Chapter 3:Unit 3.22
29. Spinetti G, Fortunato O, Caporali A, et al. MicroRNA-15a and microRNA-16 impair human circulating proangiogenic cell functions and are increased in the proangiogenic cells and serum of patients with critical limb ischemia. Circ Res 2013;112:335–346
30. Posadino AM, Cossu A, Giordo R, et al. Resveratrol alters human endothelial cells redox state and causes mitochondrial-dependent cell death. Food Chem Toxicol 2015;78:10–16
31. Fink LN, Costford SR, Lee YS, et al. Pro-inflammatory macrophages increase in skeletal muscle of high fat-fed mice and correlate with metabolic risk markers in humans. Obesity (Silver Spring) 2014;22:747–757
32. Dellavalle A, Sampaolesi M, Tonlorenzi R, et al. Pericytes of human skeletal muscle are myogenic precursors distinct from satellite cells. Nat Cell Biol 2007;9:255–267
33. Péault B, Rudnicki M, Torrente Y, et al. Stem and progenitor cells in skeletal muscle development, maintenance, and therapy. Mol Ther 2007;15:867–877
34. Nguyen N-U-N, Wang H-V. Dual roles of palladin protein in *in vitro* myogenesis: inhibition of early induction but promotion of myotube maturation. PLoS One 2015;10:e0124762
35. Meloni M, Marchetti M, Garner K, et al. Local inhibition of microRNA-24 improves reparative angiogenesis and left ventricle remodeling and function in mice with myocardial infarction. Mol Ther 2013;21:1390–1402
36. Wang JM, Tao J, Chen DD, et al. MicroRNA miR-27b rescues bone marrow-derived angiogenic cell function and accelerates wound healing in type 2 diabetes mellitus. Arterioscler Thromb Vasc Biol 2014;34:99–109
37. Caporali A, Meloni M, Völlenkle C, et al. Deregulation of microRNA-503 contributes to diabetes mellitus-induced impairment of endothelial function and reparative angiogenesis after limb ischemia. Circulation 2011;123:282–291
38. Mayo JN, Bearden SE. Driving the hypoxia-inducible pathway in human pericytes promotes vascular density in an exosome-dependent manner. Microcirculation 2015;22:711–723
39. Paneni F, Mocharla P, Akhmedov A, et al. Gene silencing of the mitochondrial adaptor p66(Shc) suppresses vascular hyperglycemic memory in diabetes. Circ Res 2012;111:278–289
40. Mehta NK, Mehta KD. Protein kinase C-beta: an emerging connection between nutrient excess and obesity. Biochim Biophys Acta 2014;1841:1491–1497
41. Liu Y, Jin J, Qiao S, et al. Inhibition of PKCβ2 overexpression ameliorates myocardial ischaemia/reperfusion injury in diabetic rats via restoring caveolin-3/Akt signaling. Clin Sci (Lond) 2015;129:331–344
42. Uezumi A, Fukada S, Yamamoto N, Takeda S, Tsuchida K. Mesenchymal progenitors distinct from satellite cells contribute to ectopic fat cell formation in skeletal muscle. Nat Cell Biol 2010;12:143–152
43. Röckl KS, Hirshman MF, Brandauer J, Fujii N, Witters LA, Goodyear LJ. Skeletal muscle adaptation to exercise training: AMP-activated protein kinase mediates muscle fiber type shift. Diabetes 2007;56:2062–2069
44. Heinonen SE, Genové G, Bengtsson E, et al. Animal models of diabetic macrovascular complications: key players in the development of new therapeutic approaches. J Diabetes Res 2015;2015:404085
45. Abou-Khalil R, Mounier R, Chazaud B. Regulation of myogenic stem cell behaviour by vessel cells: the "ménage à trois" of satellite cells, periendothelial cells and endothelial cells. Cell Cycle 2010;9:892–896
46. Caporali A, Meloni M, Nailor A, et al. p75(NTR)-dependent activation of NF-κB regulates microRNA-503 transcription and pericyte-endothelial crosstalk in diabetes after limb ischaemia. Nat Commun 2015;6:8024
47. Giorgio M, Berry A, Berniakovich I, et al. The p66Shc knocked out mice are short lived under natural condition. Aging Cell 2012;11:162–168
48. Xia Z, Kuo KH, Nagareddy PR, et al. N-acetylcysteine attenuates PKCbeta2 overexpression and myocardial hypertrophy in streptozotocin-induced diabetic rats. Cardiovasc Res 2007;73:770–782
49. Liu Y, Lei S, Gao X, et al. PKCβ inhibition with ruboxistaurin reduces oxidative stress and attenuates left ventricular hypertrophy and dysfunction in rats with streptozotocin-induced diabetes. Clin Sci (Lond) 2012;122:161–173
50. Cook NR, Albert CM, Gaziano JM, et al. A randomized factorial trial of vitamins C and E and beta carotene in the secondary prevention of cardiovascular events in women: results from the Women's Antioxidant Cardiovascular Study. Arch Intern Med 2007;167:1610–1618